

SARA: Controllable Makeup Transfer with Spatial Alignment and Region-Adaptive Normalization

Xiaojing Zhong[†], Xinyi Huang[†], Zhonghua Wu, Guosheng Lin*, Qingyao Wu*

Abstract—Makeup transfer is a process of transferring the makeup style from a reference image to the source images, while preserving the source images’ identities. This technique is highly desirable and finds many applications. However, existing methods lack fine-level control of the makeup style, making it challenging to achieve high-quality results when dealing with large spatial misalignments. To address this problem, we propose a novel Spatial Alignment and Region-Adaptive normalization method (SARA) in this paper. Our method generates detailed makeup transfer results that can handle large spatial misalignments and achieve part-specific and shade-controllable makeup transfer. Specifically, SARA comprises three modules: Firstly, a spatial alignment module that preserves the spatial context of makeup and provides a target semantic map for guiding the shape-independent style codes. Secondly, a region-adaptive normalization module that decouples shape and makeup style using per-region encoding and normalization, which facilitates the elimination of spatial misalignments. Lastly, a makeup fusion module blends identity features and makeup style by injecting learned scale and bias parameters. Experimental results show that our SARA method outperforms existing methods and achieves state-of-the-art performance on two public datasets.

Index Terms—Makeup transfer, Style transfer, Generative models, Correspondence matching, Normalization.

I. INTRODUCTION

GIVEN a facial image with a certain makeup style, the makeup transfer task aims to transfer the style to a target face. This is widely demanded in many real-world scenarios where users would like to beautify themselves. Although makeup and non-makeup images can be easily obtained from the internet, it is not easy to obtain paired images because an absolutely identical face equipped with different makeup styles is unavailable. To address this issue, one possible way [1]–[4] is to capitalize on the idea of CycleGAN [5] to construct the training in a cyclic manner by bridging two networks, one that transfers makeup styles and another that removes makeup.

However, existing makeup transfer approaches often treat different semantic regions equally, which can limit fine-grained control over makeup styles - an essential factor in achieving realistic makeup transfer results. Recent advancements [7]–[10] in style transfer, such as the control of affine transformation

[†]Co-first author.

*Corresponding author.

Xiaojing Zhong, Xinyi Huang and Qingyao Wu are with School of Software Engineering, South China University of Technology, Guangzhou, China. (email: vxj12@gmail.com, 202221045993@mail.scut.edu.cn, qyw@scut.edu.cn)

Zhonghua Wu and Guosheng Lin are with School of Computer Science and Engineering, Nanyang Technological University, Singapore. (email: zhonghua001@e.ntu.edu.sg, gslin@ntu.edu.sg)

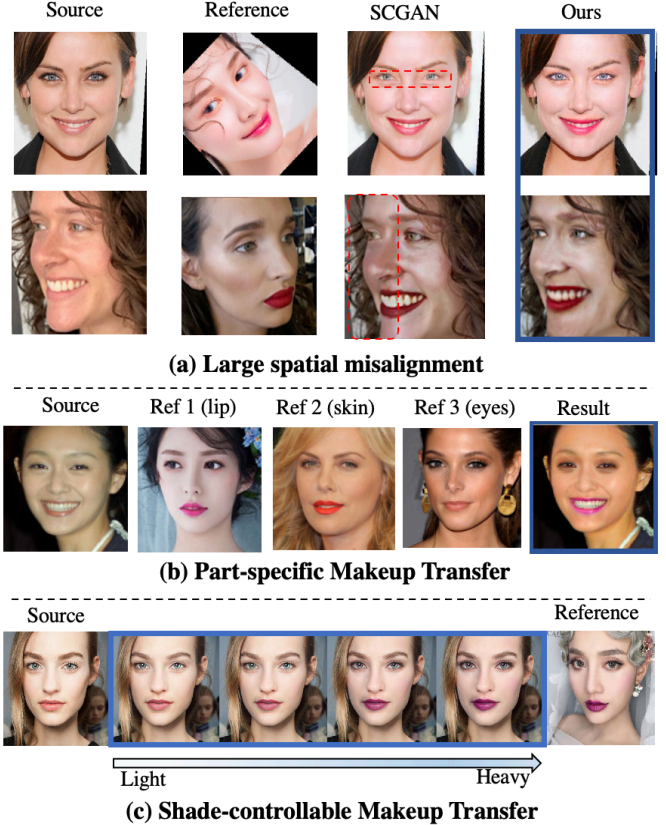


Fig. 1: SARA supports flexible operations. (a) Compared to SCGAN [6], SARA better deals with large spatial misalignment by incorporating spatial information into the transfer framework. The highlights are the unnatural results generated by SCGAN. (b) Users are allowed to select partial makeup styles from various reference images. (c) SARA can adjust the degree of the transferred makeup styles.

parameters in AdaIN layers [11], have shown great potential in virtual try-on applications [12]–[14], and we believe that these techniques can be extended to virtual makeup transfer as well. For example, Deng *et al* [6] propose a method for separating semantic regions and arranging corresponding style codes to empower AdaIN layers with spatial control. However, a decoupling of shape and style without proper preservation of spatial context can result in unnatural-looking makeup transfer (as seen in Fig. 1). [15], [16] compute the local correlation of key facial landmarks, but the resulting attention map is often too sparse to handle complex makeup styles.

Method	Property			
	Shade	Part	Misalign	Landmarks free
BGAN [1]	✗	✗	✗	✓
BGlow [17]	✓	✗	✗	✓
LADN [18]	✓	✗	✗	✗
PSGAN [15]	✓	✓	✓	✗
PSGAN++ [16]	✓	✓	✓	✗
SSAT [19]	✓	✓	✗	✓
Ours	✓	✓	✓	✓

TABLE I: "Shade" refers to methods that allow for the control of makeup shade during transfer. "Part" indicates the ability to perform partial transfer. "Misalign" refers to methods that are robust even when there is a significant spatial misalignment between the source and reference images. "Landmarks free" describes methods that can perform makeup transfer without relying on facial landmarks.

To overcome the mentioned limitations, we propose a novel makeup transfer framework called Controllable Makeup Transfer with **S**patial **A**lignment and **R**egion-Adaptive normalization (**SARA**), which comprises three modules.

First, a Spatial Alignment Module (**SAM**) is introduced to warp the reference image (with makeup) to be aligned with the source image (with non-makeup) to preserve the spatial context relationship. The matching correspondence is densely calculated in a pixel-to-pixel manner, beneficial for dealing with the makeup over a large area. Besides, the computed correspondence matrix is also used to generate the target semantic map, which serves as the broadcast mask in the following normalization. Due to the fact that the coupling of the shape and style of makeup is not conducive to accurate transfer, a Region-Adaptive normalization Module (**RAM**) is proposed to extract the per-region styles from the reference image and broadcast the style codes to the target semantic map. By incorporating the aligned features generated from SAM, RAM dynamically combines the shape-independent styles with the spatial context. Final, a Makeup Fusion Module (**MFM**) is responsible for allocating the learned scale and bias parameters to the fusion blocks, progressively fusing the identity features with the makeup styles to render the fine-grained results.

Overall, SARA is capable of achieving flexible makeup transfer controls within one unified framework. (i) SARA can deal with different poses and expressions between reference and source images, while many existing methods merely work well on frontal facial images and the same expressions. (ii) SARA can perform high-quality makeup removal when the reference and source images are inverse. (iii) SARA can realize partial makeup transfer in the scenario where users would like to transfer one part, such as the lip or eyebrows. (iv) SARA can adjust the degree of makeup styles from light to heavy. Tab I demonstrates the properties of various makeup transfer methods in summary.

Our contributions can be summarized as follows:

- We design a unified framework **SARA** for the controllable makeup transfer tasks, which supports partial, shade-control makeup transfer and removal at the same time. With our carefully designed three main modules,

our proposed SARA achieves state-of-the-art performance on the MT and M-wild datasets.

- We propose to incorporate spatial alignment into region-adaptive normalization to simultaneously eliminate the spatial gap between the reference style and the source identity and preserve the spatial context relationship.
- We estimate a correspondence matrix in a pixel-to-pixel manner to realize the spatial alignment, which is dense enough to represent detailed makeup styles. The matrix is also used to guide the style codes broadcasted to the target semantic region.

II. RELATED WORK

A. Makeup Transfer

Makeup transfer has gained significant interest in the last decade [20]–[23], with several methods proposed for transferring makeup styles from reference images to source images. Some of the popular methods include CycleGAN [5], which is an influential method for learning domain-to-domain translation, but it lacks direct constraints between input and output images, and PairedCycleGAN [2], which extends CycleGAN by introducing a paired cycle GAN for makeup transfer and removal. Li *et al.* tackle the problem by designing a dual input/output GAN to train makeup transfer and removal jointly [1]. They also propose to measure similarity by matching the color histograms of makeup regions between images.

Other studies, such as [18], [24], focus on dramatic makeup styles, while Iyu *et al.* introduce a 3D-aware GAN to unwarp the texture of the face and refine it based on the symmetry of the face to solve the shadow and occlusion problem [25]. Wan *et al.* improve the fidelity of local regions sensitive to color by consolidating the transformer architecture into makeup transfer [26], and [19] facilitates the render quality in the correct position. However, these methods lack user control over the transfer process. To address this, Chen *et al.* propose BeautyGlow [17] to disentangle makeup style and facial identity of latent vectors, enabling flexible control of style degree. PSGAN [15] and improved PSGAN++ [16] propose to handle the spatial misalignment problem facing non-frontal images by incorporating visual appearances and locations into the attention mechanism. Our proposed method, SARA, performs better in several aspects. First, we depart from the need for facial landmarks that are easily inaccurate and computational-expensive. Second, local correspondence cannot model the global context relationship. EleGant [27] uses a pyramid structure with a high-resolution feature map to preserve high-frequency makeup features beyond color distributions, but it lacks careful consideration of large misalignment. SCGAN [6] separates facial component attributes via semantic layouts, which are mapped into latent space and recombined in a specific order. However, decoupling the shape and style of makeup without any consideration of space may lead to unnatural artifacts [28], [29]. Therefore, we propose incorporating spatial alignment to retain the context that provides details.

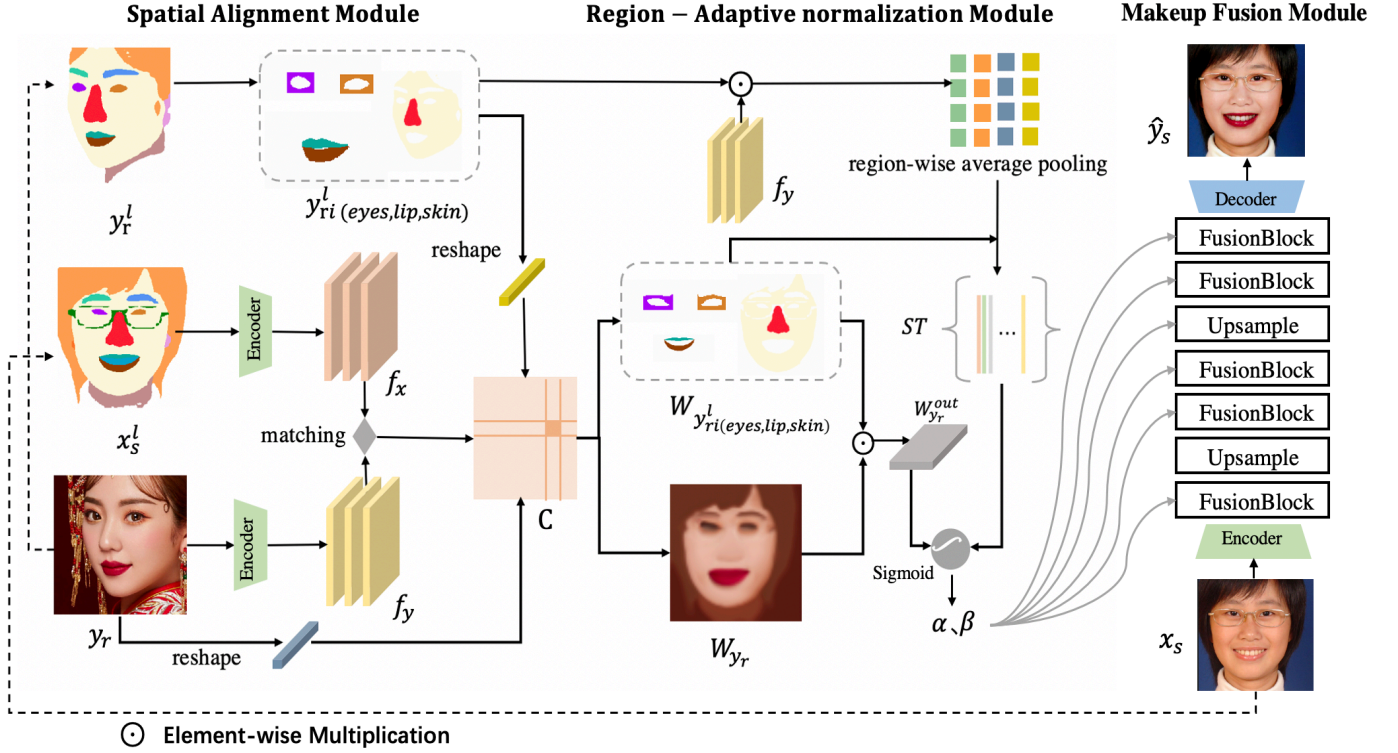


Fig. 2: **Overview of our proposed method.** It mainly has three modules: (i) Spatial Alignment Module (**SAM**) warps the reference image y_r and the partial reference semantic map y_{ri}^l to be aligned with x_s^l through estimating the dense correspondence between y_r and the source semantic map x_s^l , where $i = \{lip, skin, eyes\}$. (ii) Region-Adaptive normalization Module (**RAM**) decouples the shape and style of makeup via a region-wise average pooling layer, broadcasting the shape-independent style codes to the target semantic map $W_{y_{ri}^l}$ to generate the style matrix ST . Besides, it incorporates $W_{y_r}^{out}$ into the normalization, which provides spatial context relationship during the transfer. (iii) Makeup Fusion Module (**MFM**) modulates scale and bias parameters of the fusion blocks in multi-level, progressively fusing makeup styles with the identity features, to generate the fine-grained result \hat{y}_s .

B. Style Transfer

Conventional style transfer methods rely on hand-crafted algorithms to render an image in fixed styles [30], [31], or match two images with hand-crafting features [32], [33]. More recent advances in style transfer have shifted towards the use of deep learning techniques, specifically the increasingly effective generative models [34]–[36]. AdaIN [11] and DIN [37] use conditional instance normalization to align content and style feature statistics, but dynamic generation of affine parameters may cause distortion artifacts. Other methods use an autoencoder-based framework with feature transformation and/or fusion [8], [38]–[40]. These models have shown impressive results in generating realistic images in a given style or transferring the style of one image onto another [41]. Importantly, controlling the output of style transfer is vital for downstream applications. One approach is to decompose the global attributes of images, such as hue, saturation, and luminance [42]. In contrast to global style control, another sort of style control is spatial [43], [44], which lets the user specify which areas of the output should be rendered exclusively with features from a hand-picked region of the style image. Despite that, there exists a gap between the generated and ideal results

when applying existing style transfer methods for makeup transfer, as the latter are sensitive to semantic details and require more exquisite control.

III. METHODOLOGY

A. Problem Formulation and Notations

Let X and Y denote the domain of the images with non-makeup and the images with makeup, respectively. Given a source image $x_s \in X$ and a reference image $y_r \in Y$, our goal is to learn a mapping function: $f(x_s, y_r \rightarrow \hat{y}_s)$, where \hat{y}_s has the same makeup style as y_r while preserving the facial identity of x_s . Furthermore, as makeup removal is a special case of makeup transfer, we also learn a mapping function: $\hat{f}(y_r, x_s \rightarrow \hat{x}_r)$, where \hat{x}_r has the same makeup style as x_s while preserving the facial identity of y_r .

B. Network Structure

The overall framework of SARA is shown in Fig. 2, which consists of three modules: a Spatial Alignment Module (**SAM**), a Region-Adaptive normalization Module (**RAM**) and a Makeup Fusion Module (**MFM**). The content of each module will be introduced in detail (Sec III-B1 ~ Sec III-B3). The

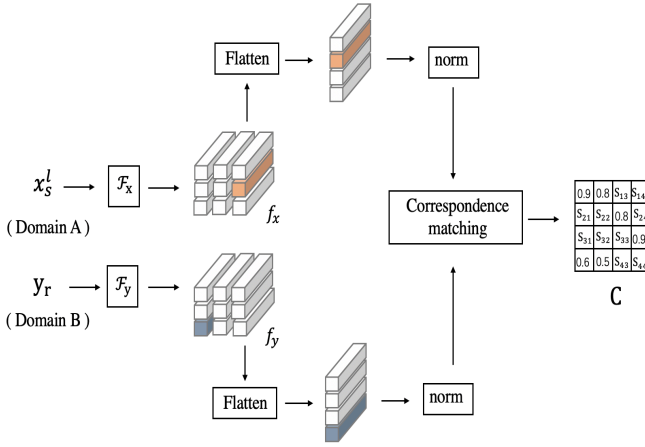


Fig. 3: Illustration of the correspondence matching process. \mathcal{F}_x and \mathcal{F}_y refer to the feature extraction operators in x_s^l and y_r , respectively. Then we flatten the generated high-level features f_x and f_y and further normalize them along the channel dimension. We estimate the dense correspondence matrix $C \in \mathbb{R}^{HW \times HW}$ through the multiplication of matrices, also regarded as the attention map.

objective functions of the whole model will be described in Sec III-C.

1) *Spatial Alignment Module*: The spatial context relationship retains fine-level details of the makeup style and should not be disregarded during the transfer. Warping the reference style to be aligned with the source identity preserves the spatial context while mitigating the spatial misalignment. SAM starts with a reference image y_r and a source semantic map x_s^l , which is obtained by running an off-the-shelf face parsing network [45] on x_s . We estimate a dense correspondence matrix between them. Fig. 3 shows the process of correspondence matching.

To be specific, we adopt two independent feature extraction operators, $\mathcal{F}_x(x_s^l)$ and $\mathcal{F}_y(y_r)$, to obtain high-level features $f_x \in \mathbb{R}^{H \times W \times C}$ and $f_y \in \mathbb{R}^{H \times W \times C}$, respectively. We leverage cosine similarity to match the aggregated features, which has been proven useful in calculating pixel-wise semantic relevance [46], [47]. Then we flatten f_x and f_y to be $f'_x \in \mathbb{R}^{C \times HW}$ and $f'_y \in \mathbb{R}^{C \times HW}$, respectively. Following the same setting as [48], the correspondence matrix $C \in \mathbb{R}^{HW \times HW}$ can be computed as:

$$C(i, j) = \frac{(f'_x(i) - u_x)^T (f'_y(j) - u_y)}{\| (f'_x(i) - u_x) \| \| (f'_y(j) - u_y) \|}, \quad (1)$$

where u_x and u_y represent the corresponding mean vectors along the channel dimension. i and j represent $f'_x(i)$ at position i and $f'_y(j)$ at position j .

Accordingly, SAM is able to warp y_r under the guidance of the dense correspondence matrix C . The warped image $W_{y_r}(u)$ can be represented as:

$$W_{y_r}(u) = \sum_v \text{softmax}_v(\alpha C(u, v) \cdot y_r(v)), \quad (2)$$

α is a hyper-parameter that controls result sharpness and is set at 100.

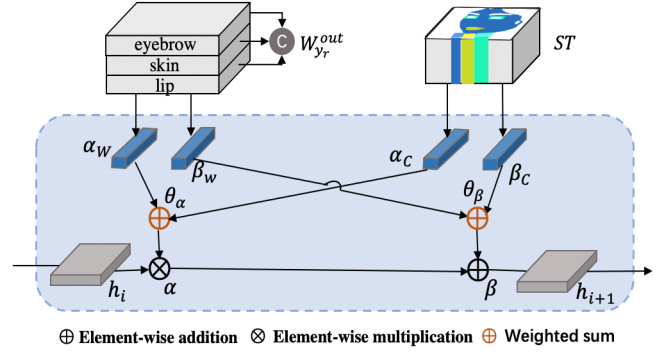


Fig. 4: Details of region-adaptive normalization. The scale and bias parameters α and β are weighted from the combined warped out $W_{y_r}^{out}$ and the style matrix ST .

Rather than using the global makeup style, we extract three specific components of W_{y_r} , which are used for embodying makeup generally, to realize partial makeup transfer. To extract the corresponding regions, we warp the partial semantic mask $y_{r_i}^l$ as below:

$$W_{y_{r_i}^l}(u) = \sum_v \text{softmax}_v(\alpha C(u, v) \cdot y_{r_i}^l(v)), \quad (3)$$

where $i = \{lip, skin, eyes\}$. The filtered makeup regions can be obtained as follows:

$$W_{y_r}^{out} = W_{y_{r_i}^l} \odot W_{y_r} \quad (4)$$

where \odot denotes element-wise multiplication for each pixel. Besides, $W_{y_{r_i}^l}$ is utilized to aid in the target semantic generation in the per-region normalization. SAM is able to warp the makeup region that covers a large area, like blush, since it models the global correspondence.

2) *Region-Adaptive normalization Module*: Style can be regarded as the embedded codes to be filled into the affine transformation parameters of the normalization [6], [7], [12], [49], independent of shape. The decoupling of shape and style contributes to the high-quality color transfer of the makeup. Inspired by [49], we takes the per-region styles extracted from the source appearance and then broadcast them to the target semantic regions on each facial part, which can be solved by per-region encoding and normalization, respectively.

Per-region encoding. We adopt the reference features F_r obtained from the spatial alignment module instead of the original reference image y_r as input. Intuitively, we contend that this could serve in maintaining the consistency and continuity of the original features since using external data may break it. To extract per-region style codes, we construct a style matrix $ST \in \mathbb{R}^{256 \times s}$ through conducting a region-wise average pooling layer on the F_r , where s denotes the dimensional concatenation of lip, skin and eyebrow. Each column of the matrix corresponds to the style code of a semantic region. We further broadcast the style codes to their target region to generate the target style map.

Per-region normalization. To be specific, we set $h^i \in \mathbb{R}^{B \times C^i \times H^i \times W^i}$ as the activation value before the i -th normalization layer, where B, C^i, H^i, W^i represent batch size,

number of channels, height and width of the i -th feature map respectively. The mean μ_c^i and standard deviation σ_c^i are calculated in the channel-wise manner. Then, the output of RAM in the i -th layer is given by:

$$h_{b,c,h,w}^{i+1} = \alpha_{c,h,w}^i \frac{h_{b,c,h,w}^i - \mu_c^i}{\sigma_c^i} + \beta_{c,h,w}^i, \quad (5)$$

where $\alpha_{c,h,w}^i$ and $\beta_{c,h,w}^i$ are the learnable parameters. As shown in the Fig. 4, they are the weighted sum of these features from the convolution output of the combined warped out $W_{y_r}^{out}$ and the style matrix ST , which are defined as:

$$\begin{aligned} \alpha_{c,h,w}^i &= \theta_\alpha \cdot \alpha_W + (1 - \theta_\alpha) \cdot \alpha_C \\ \beta_{c,h,w}^i &= \theta_\beta \cdot \beta_W + (1 - \theta_\beta) \cdot \beta_C, \end{aligned} \quad (6)$$

where θ_α and θ_β are the adaptation coefficients that are dynamically weighted from two sources in the transfer.

Different from [49], which weights the θ_α and θ_β from the style matrix and the semantic mask, we incorporate the spatial alignment into the per-region normalization, using the warped image aligned with the source identity to provide the spatial context of the style.

3) *Makeup Fusion Module*: The MFM is composed of a face identity encoder, two upsample layers, five fusion blocks, and a decoder. Compared to [38], [49], which begins with random noises, the face identity encoder is expected to extract the identity feature of x_s . Fusion blocks receive scale and bias parameters from RAM to denormalize the feature maps, and the upsample layers are used to recover the resolution of the original image. Finally, the decoder is responsible for decoding the feature maps to generate the result \hat{y}_s .

C. Loss Function

We train our model in a collaborative fashion to ensure that the various components of the network work together to maximum effect. The total loss \mathcal{L}_{total} can be defined as below:

$$\begin{aligned} \mathcal{L}_{total} &= \lambda_1 \mathcal{L}_{domain} + \lambda_2 \mathcal{L}_{perc} + \lambda_3 \mathcal{L}_{corr} \\ &+ \lambda_4 \mathcal{L}_{makeup} + \lambda_5 \mathcal{L}_{cycle} + \lambda_6 \mathcal{L}_{adv} + \lambda_7 \mathcal{L}_{id}, \end{aligned} \quad (7)$$

where $\lambda_{1,2,4,5,6,7}$ are the hyper-parameters to control the weights of each term.

Domain alignment loss. To support the correspondence learning across two different domains, we need to ensure that the feature embeddings f_x from $F_x(x_s^l)$ and f_y from $F_y(y_r)$ lie in the same domain. \mathcal{L}_{domain} can be defined as below:

$$\mathcal{L}_{domain} = \|F_x(x_s^l) - F_y(y_r)\|_1, \quad (8)$$

where $\|\cdot\|_1$ is the L1-Norm. Please note that even if $F_x(x_s^l) = F_y(y_r)$ in, we can still calculate the similarity between them to get the correspondence matrix.

Perceptual loss. High-level features usually contain semantic information. Thus, we utilize VGG-19 pretrained model [50] to extract features from the generated output \hat{y}_s and the input source image x_s , respectively. We merely adopt the activation after *relu4_2* layer which is set as ϕ_l since \hat{y}_s and x_s are not aligned in pixel-level, \mathcal{L}_{perc} can be formulated as below:

$$\mathcal{L}_{perc} = \|\phi_l(\hat{y}_s) - \phi_l(x_s)\|_2, \quad (9)$$

where $\|\cdot\|_2$ is the L2-Norm.

Correspondence regularization. Despite the domain alignment loss, there lacks a powerful supervision to train correspondence learning indeed. To solve that, we can construct a cyclic warping as [48] to ensure the learned correspondence is cycle-consistent. We warp W_{y_r} again with the correspondence matrix to conduct L1 loss with the original image y_r . \mathcal{L}_{corr} can be computed as below:

$$\mathcal{L}_{corr} = \|\hat{W}_{y_r} - y_r\|_1, \quad (10)$$

where $\hat{W}_{y_r}(u) = \sum_v softmax(\alpha C(u, v) \cdot W_{y_r}(v))$.

Adversarial loss. We adopt a discriminator [51] to constrain the latent space of output into the data distribution like y_r in order to improve the quality of the generated image \hat{y}_s . \mathcal{L}_{GAN}^G and \mathcal{L}_{GAN}^D are respectively formulated as below:

$$\begin{aligned} \mathcal{L}_{GAN}^D &= -\mathbb{E}[h(D(y))] - \mathbb{E}[h(-D(G(x, y)))] \\ \mathcal{L}_{GAN}^G &= -\mathbb{E}[D(G(x, y))], \end{aligned} \quad (11)$$

where the hinge function $h(t) = \min(0, -1 + t)$ is expected to regularize the discriminator [52], [53].

Makeup loss. It is normally used to match the local histogram of the makeup region (skin, lip and eyes) between the generated image and the pseudo ground truth proposed by [1]. We denote the pseudo ground truth that has the identity of x while equipping with the similar color distribution of y as $HM(x, y)$. The opposite is $HM(y, x)$.

\mathcal{L}_{makeup} can be computed as below:

$$\begin{aligned} \mathcal{L}_{makeup} &= \|G(x, y) - HM(x, y)\|_2 \\ &+ \|G(y, x) - HM(y, x)\|_2 \end{aligned} \quad (12)$$

Cycle consistency loss. We perform a global cycle loss [5] to maintain the consistency of the mapping between two domains due to the lack of direct supervision. \mathcal{L}_{cycle} can be calculated as below:

$$\begin{aligned} \mathcal{L}_{cycle} &= \|G(G(y, x), y) - y\|_1 \\ &+ \|G(G(x, y), x) - x\|_1 \end{aligned} \quad (13)$$

Identity loss. We construct the identity loss by referring to the reference, source, and output images as the same images. This aims to maintain consistency of the identity during the generation. \mathcal{L}_{id} can be formulated as below:

$$\begin{aligned} \mathcal{L}_{id} &= \|G(x, x) - x\|_1 \\ &+ \|G(y, y) - y\|_1 \end{aligned} \quad (14)$$

IV. EXPERIMENTS

A. Network architecture

We evaluated different architectures shown in Tab II and Tab III to choose the best one. We represent the SARA architecture as 1-2-2 (the number of fusion blocks from bottom to top) and demonstrate the architecture of adding blocks and reducing blocks in two separate tables. The main differences between these architectures are the number and the order of fusion blocks. All of the architectures start with a face identity encoder and end with an image decoder. Specifically, the fusion block consists of two components arranged in

architecture	Adding Blocks				SARA
	1-3-2	1-2-3	2-2-2	0-3-3	1-2-2
step 1	Face encoder				
step 2	FusionBlock(256,256)	FusionBlock(256,256)	FusionBlock(256,256)	-	FusionBlock(256,256)
step 3	-	-	FusionBlock(256,256)	-	-
step 4	Upsample	Upsample	Upsample	Upsample	Upsample
step 5	FusionBlock(256,128)	FusionBlock(256,128)	FusionBlock(256,128)	FusionBlock(256,256)	FusionBlock(256,128)
step 6	FusionBlock(128,128)	-	-	FusionBlock(256,128)	-
step 7	FusionBlock(128,128)	FusionBlock(128,128)	FusionBlock(128,128)	FusionBlock(128,128)	FusionBlock(128,128)
step 8	Upsample	Upsample	Upsample	Upsample	Upsample
step 9	-	FusionBlock(128,128)	-	FusionBlock(128,128)	-
step 10	FusionBlock(128,64)	FusionBlock(128,64)	FusionBlock(128,64)	FusionBlock(128,64)	FusionBlock(128,64)
step 11	FusionBlock(64,64)	FusionBlock(64,64)	FusionBlock(64,64)	FusionBlock(64,64)	FusionBlock(64,64)
step 12	Decoder	Decoder	Decoder	Decoder	Decoder

TABLE II: Adding one fusion block in 1-2-2 architecture (The number of fusion blocks from bottom to top) with different orders.

architecture	Reducing Blocks				SARA
	1-1-2	1-2-1	0-2-2	0-1-2	1-2-2
step 1	Face encoder				
step 2	FusionBlock(256,256)	FusionBlock(256,256)	-	-	FusionBlock(256,256)
step 3	Upsample	Upsample	Upsample	Upsample	Upsample
step 4	FusionBlock(256,128)	FusionBlock(256,128)	FusionBlock(256,128)	FusionBlock(256,128)	FusionBlock(256,128)
step 5	-	FusionBlock(128,128)	FusionBlock(128,128)	-	FusionBlock(128,128)
step 6	Upsample	Upsample	Upsample	Upsample	Upsample
step 7	FusionBlock(128,64)	FusionBlock(128,64)	FusionBlock(128,64)	FusionBlock(128,64)	FusionBlock(128,64)
step 8	FusionBlock(64,64)	-	FusionBlock(64,64)	FusionBlock(64,64)	FusionBlock(64,64)
step 9	Decoder	Decoder	Decoder	Decoder	Decoder

TABLE III: Reducing one fusion block in 1-2-2 architecture (The number of fusion blocks from bottom to top) with different orders.

sequence: a region-adaptive normalization layer, leaky ReLU activation, and spectral normalization [54]. Its final output is obtained by connecting the residual of the input and the result after normalization. The results generated by the different architectures are shown in Fig. 5. We can see that 1-2-2 gets the best makeup transfer results in terms of the eye shadow and shade. Besides, we adopt the discriminator from pix2pixHD [55].

B. Implementation Setting and datasets

Datasets. Experiments are conducted on the Makeup Transfer (MT) dataset [1]. It contains 2719 makeup images, each of which has variations in poses, expressions, and makeup styles. Besides, it contains 1115 non-makeup images with different human identities. Following [1], we randomly selected 250 makeup images and 100 non-makeup images as the testing set, and the rest as the training set. To further validate the effectiveness of our model, we also tested it in the M-wild dataset [15], in which the facial images have complex backgrounds.

Implementation Details We train the model for 40 epochs with an Adam optimizer ($\beta_1 = 0, \beta_2 = 0.9$). We set imbalanced learning rates, $1e-4$ and $4e-4$ respectively, following the TTUR. The spectral norm is used in both the generator and discriminator for stabilizing the training. All the experiments were conducted on one NVIDIA GeForce RTX 2080 Ti GPU, and it takes roughly 2 days to train the whole model when batch size is set to 1. The reason we set the batch size to 1 is because the computation of correspondences matching

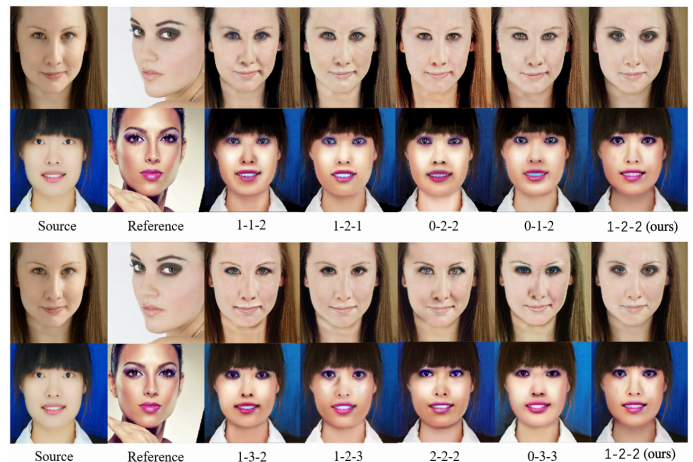


Fig. 5: **Qualitative comparisons with different architectures.** The above two lines show a comparison of different orders for adding a fusion block, while the below two lines show a comparison of different orders for reducing a fusion block.

in the spatial alignment module uses a lot of memory, and if we remove cycle loss and identity loss from the loss function, we can adjust it to a larger batch size, but it also has some impact on the results, which is a trade-off. We empirically [6], [15] set the hyper-parameters of formula 7 as ($\lambda_1=1.0, \lambda_2=0.001, \lambda_3=0.1, \lambda_4=50.0, \lambda_5=1.0, \lambda_6=10.0, \lambda_7=1.0$).



Fig. 6: **Qualitative comparison in MT dataset.** The compared methods include: **CycleGAN** [ICCV'17], **PairedCycleGAN** [CVPR'18], **BeautyGAN** [ACMMM'18], **BeautyGlow** [CVPR'19], **LADN** [ICCV'19], **PSGAN** [CVPR'20], **SCGAN** [CVPR'21], **SSAT** [AAAI'22]. SARA is able to generate more satisfactory results. Detailed analysis are elaborated in Sec IV-C.



Fig. 7: **Qualitative comparisons with open source models in M-Wild dataset.** The compared methods include: **BeautyGAN** [ACMMM'18], **PSGAN** [CVPR'20], **SCGAN** [CVPR'21], **SSAT** [AAAI'22], **EleGANt** [ECCV'22]. SARA is good at handling large misalignment. Detailed analysis are elaborated in Sec IV-C.

C. Qualitative Results

In Fig. 6, we demonstrate the visual qualitative comparisons with other models on the frontal facial images. For a fair comparison, we cropped the results of their models directly from their papers since CycleGAN [2] and BeautyGlow [17] have not released their code or pre-trained models. Both PairedCycleGAN [2] and CycleGAN modify the image domain as a whole. This only matches the skin of the face to the reference image, which can't accurately transfer lipstick and eye shadow. BeautyGAN [1] and BeautyGlow enforce the local transfer through learning makeup loss. However, the skin color generated by BeautyGlow is not close to the reference image, and the tooth texture of the reference image is incorrectly transferred to the lips (the second row). LADN [18] is designed for dramatic makeup transfer, which is not appropriate for the normal makeup style. PSGAN [15] and SCGAN [6] show better transfer results than the above methods. However, PSGAN generates an unnatural eye shadow since it mitigates the misalignment caused by local correspondence.

SCGAN transfers the makeup style by decomposing the facial attributes, which ignores the spatial layout. The background color of the image that is made is red, but the background color of the image that is used as a reference is green. This is because it is hard to tell where the background ends and the makeup begins during the transfer. Eyeshadow and lipstick generated by SSAT [19] are not bright enough. By contrast, SARA is capable of not only accurate spatial transfer but also of preserving the details of makeup style. We further evaluated SARA with other open source models on M-Wild [15] to validate its robustness under large discrepancies in expressions and poses. The results generated by EleGANt [27], shown in the first and third rows of Fig. 7, appear to have inaccurate eye shadow shapes, while those shown in the second row have unnatural facial shadows. Our method has superior spatial awareness to handle the large misalignment of makeup transfer.

Model	Align Rank 1	MisAlign Rank 1
BeautyGAN [1]	10.6%	3.1%
PSGAN [15]	15.2%	19.2%
SCGAN [6]	30.6%	28.4%
SARA (Ours)	43.6%	49.3%

TABLE IV: **User study(%) on the MT dataset.** Align Rank 1 and MisAlign Rank 1 mean that users select the best one when source images and reference images are well aligned or not.

Model	BeautyGAN	PSGAN	SCGAN	Ours
Runtime	0.1681	0.4218	0.2388	0.1523

TABLE V: **Runtime(in second).** Lower means better.

D. Quantitative Results

User study. In terms of quantitative comparison, we follow [6], [19], [27] to evaluate the quality of the makeup transfer through a user study. Note that most of the metrics used in the synthesis tasks are designed to evaluate the global image quality rather than the quality of the makeup transfer itself. We conducted a user study with 30 participants to compare our method with other methods, using the pre-trained models provided by those other methods. They are BeautyGAN, PSGAN, and SCGAN. PSGAN and SCGAN are both designed to deal with spatial misalignment, so we conducted user studies on both aligned and misaligned samples separately. A group of samples consists of four images derived from four methods, respectively. We randomly selected 15 groups of aligned samples and 15 groups of misaligned samples to ask users to rank the methods, observing the realism of the generated images and the similarity of makeup styles with the reference image. The comparison results of different methods are shown in Table IV, which indicate that our method achieves the best performance, especially with misaligned samples.

Runtime. As shown in Tab V, our model demonstrates the fastest inference speed among all the compared methods.

E. Controllable Makeup Transfer

1) *Partial Makeup Transfer:* Our makeup styles come from two sources: aligned warped out $W_y r^{out}$ and non-aligned style matrix ST . Let y_{ri} denote the reference images providing makeup style for certain parts, where $i = \{lip, skin, eyes\}$. In the inference stage, the combined $W_{y_{ri}}^{out}$ can be replaced as below:

$$W_{y_{ri}}^{out} = (W_{y_{reyes}}^l \odot W_{y_{reyes}}) + (W_{y_{rlip}}^l \odot W_{y_{rlip}}) + (W_{y_{rskin}}^l \odot W_{y_{rskin}}), \quad (15)$$

where \odot denotes element-wise multiplication for each pixel between the partial warped semantic mask and corresponding warped images. The combined style matrix ST_c can be obtained by concatenating the style codes distilled from corresponding reference features and further broadcasting the combined style code according to the combined warped semantic map. Fig. 1(b) demonstrates the partial makeup transfer when styles are obtained from the lips in *Ref 1*, the skin in *Ref 2*, and the eyes in *Ref 3*.



Fig. 8: **Makeup transfer with four reference images by linear interpolation.**

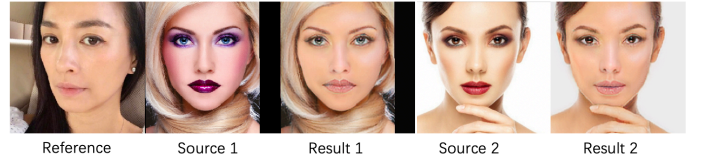


Fig. 9: **Makeup removal results.** The inverse transfer works well with SARA.

2) *Shade-controllable Makeup Transfer:* To get shade-controllable makeup transfer, we apply linear interpolation on two intermediately warped products (warped images W_{y_r} and style code ST) as below:

$$W_y = \alpha W_{y_r} + (1 - \alpha) W_{y_s} \quad (16)$$

$$ST = \alpha ST_r + (1 - \alpha) ST_s$$

The coefficient $\alpha \in [0, 1]$ in the formula controls the degree of shade. The example can be seen in the Fig. 1(c). SARA can fuse the makeup of multiple images into one source image by replacing the source image in the formula with another reference image.

$$W_y = \alpha W_{y_{r1}} + (1 - \alpha) W_{y_{r2}} \quad (17)$$

$$ST = \alpha ST_{r1} + (1 - \alpha) ST_{r2}$$

As Fig. 8 shows, when we change α from 0 to 1 with a gradient of 0.2, we can get the results of which the styles are from four reference images in varying degrees.

3) *Makeup Removal:* The process of removing makeup is similar to transferring it, except that the source and reference images are reversed. Specifically, by using a non-makeup image as the reference (y_r) and a makeup image as the source (x_s), we can achieve a makeup removal effect. Fig. 9 displays the results of our method for makeup removal, demonstrating that SARA is effective at removing makeup.



Fig. 10: **Effects of SAM.** The third column is the intermediate warped output generated from SAM. The fourth column is the generated results without using SAM. The fifth column is the generated results using SNM with SPADE but without SAM.

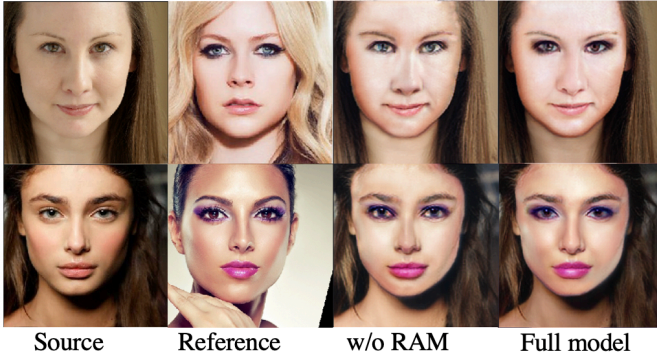


Fig. 11: **Effects of RAM.** In terms of the texture quality of style, the full model outperforms *w/o RAM*.

F. Ablation Studies

Effectiveness of the Spatial-aware Alignment Module (SAM). SAM warp the reference image to be aligned with the source image. The third column of Fig. 10 shows the immediate warped images generated by SAM, it can be seen that makeup styles can be well preserved during the warping although the results are not very sharp. *w/o SAM* denotes using the non-aligned semantic-adaptive normalization without SAM. In particular, blusher cannot be transferred while the color of lip is gloomy (first row) and artifacts of the eyes can be observed (second row). To further explore the effectiveness of SAM, we also conduct ablation experiments on combining the region-adaptive normalization with SPADE [56] like [49]. The generated results are shown in the fifth column. Although the semantic mask can mitigate the influence of unnatural artifacts, it contributes little effect on the makeup transfer. Thus, the results shown in the last column that have appropriate makeup styles are benefited by SAM.

Effectiveness of the Region-Adaptive normalization Module (RAM). RAM performs per-region normalization through adaptively fusing the makeup styles according to the warped image providing spatial context and the style matrix equipped with shape-independent style information. As shown in the Fig. 11, *w/o RAM* indicates achieving per-region encoding and normalization merely on the warped output generated from SAM. RAM steers the results to be more natural with the better texture.

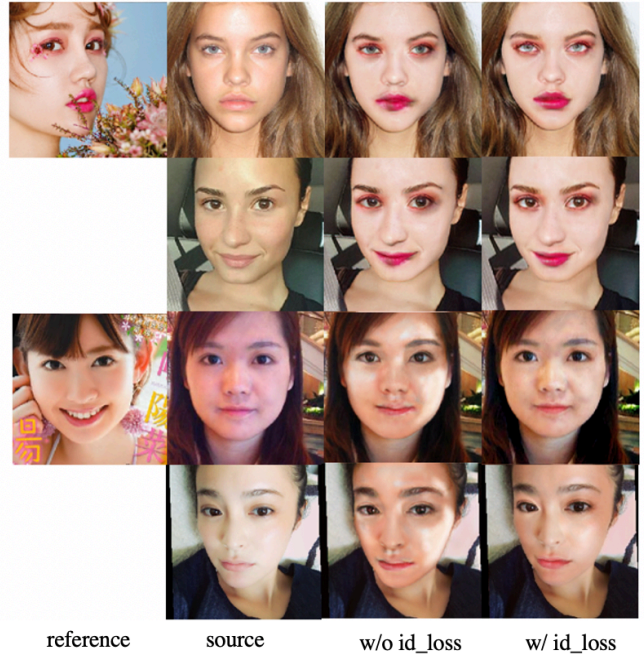


Fig. 12: **Effects of identity loss.** The occlusion in the reference image may cause artifacts in the corresponding regions, without identity loss. It can also effectively eliminate any mottled light and shadow.



Fig. 13: **Failure cases in the dataset collected by [18] with complex and dramatic styles.** The transferred texture preservation is not ideal when the reference images have large areas of camouflage or special symbols, then.

Effectiveness of the identity loss. In this paper, we introduce the identity loss to control the continuity and consistency during generation, which alleviates the production of unnatural results caused by occlusion or changes in different lighting conditions. As shown in the Fig. 12, the makeup transfer results generated from the model trained with identity loss will not be affected by the occluded lips (the first and second rows). Furthermore, when the image’s lighting with makeup is abnormal, identity loss can make the transfer result free of mottled light and shadow, leading to the natural results (the third and fourth rows). Overall, identity loss can make the model competent for some unconventional transfers.

Limitation: In terms of dramatic styles, one potential limitation of our model is that it may not be able to accurately transfer dramatic makeup looks filled with blockbuster camouflage, as shown in Fig. 13. This could be because our training data did not include enough examples of such complex

makeup designs, which may have made it difficult for the model to learn how to transfer them. In order to improve the performance of our model in this area, we would need to expand our training dataset to include a wider variety of makeup looks.

V. CONCLUSION

To solve the problem of controllable makeup transfer, we introduced SARA, a method that allows for freely transferring makeup styles. The proposed architecture decouples the shape and color of the style while retaining the spatial context relationship. We warp the partial semantic mask by correspondence matching with a reference image to preserve the spatial context rather than filling styles into non-makeup masks. Our proposed correspondence matrix is calculated in a pixel-to-pixel manner, dense enough to represent detailed and exquisite makeup styles. Eliminating spatial gaps will sacrifice the precision and sharpness of styles, leading to a smooth result.

VI. ACKNOWLEDGEMENT

This work was supported by National Natural Science Foundation of China (NSFC) 62272172, Guangdong Basic and Applied Basic Research Foundation 2023A1515012920, Tip-top Scientific and Technical Innovative Youth Talents of Guangdong Special Support Program 2019TQ05X200 and 2022 Tencent Wechat Rhino-Bird Focused Research Program (Tencent WeChat RBFR2022008), and the Major Key Project of PCL under Grant PCL2021A09.

REFERENCES

- [1] T. Li, R. Qian, C. Dong, S. Liu, Q. Yan, W. Zhu, and L. Lin, "Beautygan: Instance-level facial makeup transfer with deep generative adversarial network," in *Proceedings of the 26th ACM international conference on Multimedia*, 2018, pp. 645–653.
- [2] H. Chang, J. Lu, F. Yu, and A. Finkelstein, "Pairedcyclegan: Asymmetric style transfer for applying and removing makeup," in *Proceedings of the IEEE conference on computer vision and pattern recognition*, 2018, pp. 40–48.
- [3] Y. Choi, M. Choi, M. Kim, J.-W. Ha, S. Kim, and J. Choo, "Stargan: Unified generative adversarial networks for multi-domain image-to-image translation," in *Proceedings of the IEEE conference on computer vision and pattern recognition*, 2018, pp. 8789–8797.
- [4] X. Huang, M.-Y. Liu, S. Belongie, and J. Kautz, "Multimodal unsupervised image-to-image translation," in *Proceedings of the European conference on computer vision (ECCV)*, 2018, pp. 172–189.
- [5] J.-Y. Zhu, T. Park, P. Isola, and A. A. Efros, "Unpaired image-to-image translation using cycle-consistent adversarial networks," in *Proceedings of the IEEE international conference on computer vision*, 2017, pp. 2223–2232.
- [6] H. Deng, C. Han, H. Cai, G. Han, and S. He, "Spatially-invariant style-codes controlled makeup transfer," in *Proceedings of the IEEE/CVF Conference on Computer Vision and Pattern Recognition*, 2021, pp. 6549–6557.
- [7] J. Zhang, K. Li, Y.-K. Lai, and J. Yang, "Pise: Person image synthesis and editing with decoupled gan," in *Proceedings of the IEEE/CVF Conference on Computer Vision and Pattern Recognition*, 2021, pp. 7982–7990.
- [8] V. Dumoulin, J. Shlens, and M. Kudlur, "A learned representation for artistic style," *arXiv preprint arXiv:1610.07629*, 2016.
- [9] S. Choi, S. Park, M. Lee, and J. Choo, "Viton-hd: High-resolution virtual try-on via misalignment-aware normalization," in *Proceedings of the IEEE/CVF Conference on Computer Vision and Pattern Recognition*, 2021, pp. 14 131–14 140.
- [10] Y. Lyu, Y. Jiang, B. Peng, and J. Dong, "Infostyler: Disentanglement information bottleneck for artistic style transfer," *IEEE Transactions on Circuits and Systems for Video Technology*, 2023.
- [11] X. Huang and S. Belongie, "Arbitrary style transfer in real-time with adaptive instance normalization," in *Proceedings of the IEEE international conference on computer vision*, 2017, pp. 1501–1510.
- [12] Z. Lv, X. Li, X. Li, F. Li, T. Lin, D. He, and W. Zuo, "Learning semantic person image generation by region-adaptive normalization," in *Proceedings of the IEEE/CVF Conference on Computer Vision and Pattern Recognition*, 2021, pp. 10 806–10 815.
- [13] Y. Men, Y. Mao, Y. Jiang, W.-Y. Ma, and Z. Lian, "Controllable person image synthesis with attribute-decomposed gan," in *Proceedings of the IEEE/CVF conference on computer vision and pattern recognition*, 2020, pp. 5084–5093.
- [14] X. Zhong, Z. Wu, T. Tan, G. Lin, and Q. Wu, "Mv-ton: Memory-based video virtual try-on network," in *Proceedings of the 29th ACM International Conference on Multimedia*, 2021, pp. 908–916.
- [15] W. Jiang, S. Liu, C. Gao, J. Cao, R. He, J. Feng, and S. Yan, "Psgan: Pose and expression robust spatial-aware gan for customizable makeup transfer," in *Proceedings of the IEEE/CVF Conference on Computer Vision and Pattern Recognition*, 2020, pp. 5194–5202.
- [16] S. Liu, W. Jiang, C. Gao, R. He, J. Feng, B. Li, and S. Yan, "Psgan++: Robust detail-preserving makeup transfer and removal," *IEEE Transactions on Pattern Analysis and Machine Intelligence*, 2021.
- [17] H.-J. Chen, K.-M. Hui, S.-Y. Wang, L.-W. Tsao, H.-H. Shuai, and W.-H. Cheng, "Beautyglow: On-demand makeup transfer framework with reversible generative network," in *Proceedings of the IEEE/CVF Conference on Computer Vision and Pattern Recognition*, 2019, pp. 10 042–10 050.
- [18] Q. Gu, G. Wang, M. T. Chiu, Y.-W. Tai, and C.-K. Tang, "Ladn: Local adversarial disentangling network for facial makeup and de-makeup," in *Proceedings of the IEEE/CVF International Conference on Computer Vision*, 2019, pp. 10 481–10 490.
- [19] Z. Sun, Y. Chen, and S. Xiong, "Ssat: a symmetric semantic-aware transformer network for makeup transfer and removal," in *Proceedings of the AAAI Conference on Artificial Intelligence*, vol. 36, no. 2, 2022, pp. 2325–2334.
- [20] S. Wang and Y. Fu, "Face behind makeup," in *Thirtieth AAAI Conference on Artificial Intelligence*, 2016.
- [21] C. Li, K. Zhou, and S. Lin, "Simulating makeup through physics-based manipulation of intrinsic image layers," in *Proceedings of the IEEE Conference on Computer Vision and Pattern Recognition*, 2015, pp. 4621–4629.
- [22] Y. Li, L. Song, X. Wu, R. He, and T. Tan, "Anti-makeup: Learning a bi-level adversarial network for makeup-invariant face verification," in *Proceedings of the AAAI Conference on Artificial Intelligence*, vol. 32, no. 1, 2018.
- [23] D. Guo and T. Sim, "Digital face makeup by example," in *2009 IEEE Conference on Computer Vision and Pattern Recognition*. IEEE, 2009, pp. 73–79.
- [24] T. Nguyen, A. T. Tran, and M. Hoai, "Lipstick ain't enough: beyond color matching for in-the-wild makeup transfer," in *Proceedings of the IEEE/CVF Conference on Computer Vision and Pattern Recognition*, 2021, pp. 13 305–13 314.
- [25] Y. Lyu, J. Dong, B. Peng, W. Wang, and T. Tan, "Sogan: 3d-aware shadow and occlusion robust gan for makeup transfer," in *Proceedings of the 29th ACM International Conference on Multimedia*, 2021, pp. 3601–3609.
- [26] Z. Wan, H. Chen, J. An, W. Jiang, C. Yao, and J. Luo, "Facial attribute transformers for precise and robust makeup transfer," in *Proceedings of the IEEE/CVF Winter Conference on Applications of Computer Vision*, 2022, pp. 1717–1726.
- [27] C. Yang, W. He, Y. Xu, and Y. Gao, "Elegant: Exquisite and locally editable gan for makeup transfer," in *Computer Vision—ECCV 2022: 17th European Conference, Tel Aviv, Israel, October 23–27, 2022, Proceedings, Part XVI*. Springer, 2022, pp. 737–754.
- [28] J. Liu, X. Fan, J. Jiang, R. Liu, and Z. Luo, "Learning a deep multi-scale feature ensemble and an edge-attention guidance for image fusion," *IEEE Transactions on Circuits and Systems for Video Technology*, vol. 32, no. 1, pp. 105–119, 2021.
- [29] Z. Zhao, B. Xiong, L. Wang, Q. Ou, L. Yu, and F. Kuang, "Retinexdip: A unified deep framework for low-light image enhancement," *IEEE Transactions on Circuits and Systems for Video Technology*, vol. 32, no. 3, pp. 1076–1088, 2021.
- [30] P. Haeberli, "Paint by numbers: Abstract image representations," in *Proceedings of the 17th annual conference on Computer graphics and interactive techniques*, 1990, pp. 207–214.

- [31] A. Hertzmann, "Painterly rendering with curved brush strokes of multiple sizes," in *Proceedings of the 25th annual conference on Computer graphics and interactive techniques*, 1998, pp. 453–460.
- [32] A. Hertzmann, C. E. Jacobs, N. Oliver, B. Curless, and D. H. Salesin, "Image analogies," in *Proceedings of the 28th annual conference on Computer graphics and interactive techniques*, 2001, pp. 327–340.
- [33] A. A. Efros and W. T. Freeman, "Image quilting for texture synthesis and transfer," in *Proceedings of the 28th annual conference on Computer graphics and interactive techniques*, 2001, pp. 341–346.
- [34] W. Tang, F. He, Y. Liu, Y. Duan, and T. Si, "Datfuse: Infrared and visible image fusion via dual attention transformer," *IEEE Transactions on Circuits and Systems for Video Technology*, 2023.
- [35] W. Zhou, X. Lin, J. Lei, L. Yu, and J.-N. Hwang, "Mffenet: Multiscale feature fusion and enhancement network for rgb–thermal urban road scene parsing," *IEEE Transactions on Multimedia*, vol. 24, pp. 2526–2538, 2021.
- [36] P. Zhou, L. Xie, B. Ni, L. Liu, and Q. Tian, "Hrinversion: High-resolution gan inversion for cross-domain image synthesis," *IEEE Transactions on Circuits and Systems for Video Technology*, 2022.
- [37] Y. Jing, X. Liu, Y. Ding, X. Wang, E. Ding, M. Song, and S. Wen, "Dynamic instance normalization for arbitrary style transfer," in *Proceedings of the AAAI Conference on Artificial Intelligence*, vol. 34, no. 04, 2020, pp. 4369–4376.
- [38] D. Y. Park and K. H. Lee, "Arbitrary style transfer with style-attentional networks," in *proceedings of the IEEE/CVF conference on computer vision and pattern recognition*, 2019, pp. 5880–5888.
- [39] Y. Deng, F. Tang, W. Dong, H. Huang, C. Ma, and C. Xu, "Arbitrary video style transfer via multi-channel correlation," in *Proceedings of the AAAI Conference on Artificial Intelligence*, vol. 35, no. 2, 2021, pp. 1210–1217.
- [40] J. An, S. Huang, Y. Song, D. Dou, W. Liu, and J. Luo, "Artflow: Unbiased image style transfer via reversible neural flows," in *Proceedings of the IEEE/CVF Conference on Computer Vision and Pattern Recognition*, 2021, pp. 862–871.
- [41] H. Chen, F. Shao, X. Chai, Y. Gu, Q. Jiang, X. Meng, and Y.-S. Ho, "Quality evaluation of arbitrary style transfer: subjective study and objective metric," *IEEE Transactions on Circuits and Systems for Video Technology*, 2022.
- [42] L. A. Gatys, A. S. Ecker, M. Bethge, A. Hertzmann, and E. Shechtman, "Controlling perceptual factors in neural style transfer," in *Proceedings of the IEEE conference on computer vision and pattern recognition*, 2017, pp. 3985–3993.
- [43] M. Lu, H. Zhao, A. Yao, F. Xu, Y. Chen, and L. Zhang, "Decoder network over lightweight reconstructed feature for fast semantic style transfer," in *Proceedings of the IEEE international conference on computer vision*, 2017, pp. 2469–2477.
- [44] N. Kolkin, J. Salavon, and G. Shakhnarovich, "Style transfer by relaxed optimal transport and self-similarity," in *Proceedings of the IEEE/CVF Conference on Computer Vision and Pattern Recognition*, 2019, pp. 10 051–10 060.
- [45] Z. Wei, Y. Sun, J. Wang, H. Lai, and S. Liu, "Learning adaptive receptive fields for deep image parsing network," in *Proceedings of the IEEE conference on computer vision and pattern recognition*, 2017, pp. 2434–2442.
- [46] B. Zhang, M. He, J. Liao, P. V. Sander, L. Yuan, A. Bermak, and D. Chen, "Deep exemplar-based video colorization," in *Proceedings of the IEEE/CVF Conference on Computer Vision and Pattern Recognition*, 2019, pp. 8052–8061.
- [47] C. Luo, J. Zhan, X. Xue, L. Wang, R. Ren, and Q. Yang, "Cosine normalization: Using cosine similarity instead of dot product in neural networks," in *International Conference on Artificial Neural Networks*. Springer, 2018, pp. 382–391.
- [48] P. Zhang, B. Zhang, D. Chen, L. Yuan, and F. Wen, "Cross-domain correspondence learning for exemplar-based image translation," in *Proceedings of the IEEE/CVF Conference on Computer Vision and Pattern Recognition*, 2020, pp. 5143–5153.
- [49] P. Zhu, R. Abdal, Y. Qin, and P. Wonka, "Sean: Image synthesis with semantic region-adaptive normalization," in *Proceedings of the IEEE/CVF Conference on Computer Vision and Pattern Recognition*, 2020, pp. 5104–5113.
- [50] K. Simonyan and A. Zisserman, "Very deep convolutional networks for large-scale image recognition," *arXiv preprint arXiv:1409.1556*, 2014.
- [51] M. Mirza and S. Osindero, "Conditional generative adversarial nets," *arXiv preprint arXiv:1411.1784*, 2014.
- [52] H. Zhang, I. Goodfellow, D. Metaxas, and A. Odena, "Self-attention generative adversarial networks," in *International conference on machine learning*. PMLR, 2019, pp. 7354–7363.
- [53] A. Brock, J. Donahue, and K. Simonyan, "Large scale gan training for high fidelity natural image synthesis," *arXiv preprint arXiv:1809.11096*, 2018.
- [54] T. Miyato, T. Kataoka, M. Koyama, and Y. Yoshida, "Spectral normalization for generative adversarial networks," *arXiv preprint arXiv:1802.05957*, 2018.
- [55] T.-C. Wang, M.-Y. Liu, J.-Y. Zhu, A. Tao, J. Kautz, and B. Catanzaro, "High-resolution image synthesis and semantic manipulation with conditional gans," in *Proceedings of the IEEE conference on computer vision and pattern recognition*, 2018, pp. 8798–8807.
- [56] T. Park, M.-Y. Liu, T.-C. Wang, and J.-Y. Zhu, "Semantic image synthesis with spatially-adaptive normalization," in *Proceedings of the IEEE/CVF conference on computer vision and pattern recognition*, 2019, pp. 2337–2346.

Supplementary Material

This supplementary material contains more details of the network, including the architecture, more training details and more additional qualitative results in our paper ‘‘SARA: Controllable Makeup Transfer with Spatial Alignment and Region-Adaptive Normalization’’.

We represent the SARA architecture as 1-2-2 (the number of fusion blocks from bottom to top) and demonstrate the architecture of adding blocks and reducing blocks in two separate tables. The main differences between these architectures are the number and the order of fusion blocks. All of the architectures start with a face identity encoder and end with an image decoder. Specifically, the fusion block consists of two components arranged in sequence: a region-adaptive normalization layer, leaky ReLU activation, and spectral normalization [?]. Its final output is obtained by connecting the residual of the input and the result after normalization. The results generated by the different architectures are shown in ???. We can see that 1-2-2 gets the best makeup transfer results in terms of the eye shadow and shade. Besides, we adopt the discriminator from pix2pixHD [?].

SSIM & FID. Generative tasks have incorporated the use of Structural SIMilarity (SSIM) as a metric [?], [?], [?]. SSIM is a numerical measure that takes into account the luminance, contrast, and structure of an image. The FID (Fréchet Inception Distance) is a metric used to evaluate the quality of generated images compared to real images. To compute FID, both the generated and real images are passed through a pre-trained InceptionV3 model [?]. Please note that SSIM and FID are not suitable for transfer tasks because these metrics are designed to evaluate the quality of generated images and do not consider the effectiveness of the makeup transfer [?]. Therefore, higher SSIM scores and lower FID scores do not necessarily indicate better transfer results. The comparison results of different methods and architectures are shown in Tab III, which shows that our full model has a good effect in terms of the quality of generated images.

A. Details of Using Optical Flow

As we have discussed in our main paper, optical flow is optional to add into our network, and applying flow cues to our network is straightforward. First of all, let us first introduce why optical flow can help us. As is shown in Fig ??, when we directly use the optical flow as input, the output predictions are comparable. This is because the optical flows reflect the foreground moving salient objects without any complicated backgrounds, and thus, our network can well extract their features and yields the masks. Based on this, we consider that combing the optical flow features with the origin image feature can help the network focus on more foreground salient objects. Fig ?? shows us the overall architecture of using the optical flow information. Specifically, we maintain the transformer block, intra-MLP learning module, and decoder unchanged but slightly modify the encoder features. We take both the optical flows generated by FlowNet2.0 [?] and adjacent frames as input, and they share the same encoder. The enhanced features of the

group-based images to be fed into the subsequent network can be formulated as:

$$\begin{aligned} F_{3_img} &= F_{3_flow} \times F_{3_img}, \\ F_{4_img} &= F_{4_flow} \times F_{4_img}. \end{aligned} \quad (8)$$

This operation enables the image features to pay more attention to the targeted regions by combining flow cues regardless of the distracting background items. Note that our method of using optical flow may not be the optimal way, maybe using a separate optical flow branch and a unique combination can further improve the network performance. However, using the optical flow is not our framework’s main purpose and contribution, we can already achieve state-of-the-art performance on three benchmarks (*i.e.*, FBMS [?], ViSal [?] and SegV2 [?]) without using it. We will continue to refine and research possible ways to improve our network in future work.

B. More Training Details

For object co-segmentation (CoS) and co-saliency detection (CoSD), unlike the previous methods (*i.e.*, GCAGC [?], CADC [?]) that are trained on both COCO-SEG [?] and other saliency datasets (*i.e.*, MSRA-B [?], DUTS [?]), we train our method only using COCO-SEG [?] dataset and without using data augmentation like copy-and-paste in CADC [?], Jigsaw in GICD [?]. For video salient object detection (VSOD), we follow the previous works (*i.e.*, FSNet [?], PCSA [?]) that employ the random flip, random rotation and multi-scale {0.75, 1, 1.25} training strategy in the training phase.

C. More Visualizations

Matching. To further provide the network interpretability, we visualize how group-based images match features with each other during network learning. Fig ?? shows the highly correlated patches in different images, which illustrates that our network can well capture the object similarities and discover the object regions.

Fig ?? and Fig ?? show more visualizations on co-Segmentation and co-saliency detection tasks. More other full predicted results including video salient object detection can be found and downloaded in our project page: <https://github.com/suyukun666/UFO>.

architecture	Adding Blocks				SARA
	1-3-2	1-2-3	2-2-2	0-3-3	1-2-2
step 1	Face encoder				
step 2	FusionBlock(256,256)	FusionBlock(256,256)	FusionBlock(256,256)	-	FusionBlock(256,256)
step 3	-	-	FusionBlock(256,256)	-	-
step 4	Upsample	Upsample	Upsample	Upsample	Upsample
step 5	FusionBlock(256,128)	FusionBlock(256,128)	FusionBlock(256,128)	FusionBlock(256,256)	FusionBlock(256,128)
step 6	FusionBlock(128,128)	-	-	FusionBlock(256,128)	-
step 7	FusionBlock(128,128)	FusionBlock(128,128)	FusionBlock(128,128)	FusionBlock(128,128)	FusionBlock(128,128)
step 8	Upsample	Upsample	Upsample	Upsample	Upsample
step 9	-	FusionBlock(128,128)	-	FusionBlock(128,128)	-
step 10	FusionBlock(128,64)	FusionBlock(128,64)	FusionBlock(128,64)	FusionBlock(128,64)	FusionBlock(128,64)
step 11	FusionBlock(64,64)	FusionBlock(64,64)	FusionBlock(64,64)	FusionBlock(64,64)	FusionBlock(64,64)
step 12	Decoder	Decoder	Decoder	Decoder	Decoder

TABLE I: Adding one fusion block in 1-2-2 architecture(The number of fusion blocks from bottom to top) with different orders.

architecture	Reducing Blocks				SARA
	1-1-2	1-2-1	0-2-2	0-1-2	1-2-2
step 1	Face encoder				
step 2	FusionBlock(256,256)	FusionBlock(256,256)	-	-	FusionBlock(256,256)
step 3	Upsample	Upsample	Upsample	Upsample	Upsample
step 4	FusionBlock(256,128)	FusionBlock(256,128)	FusionBlock(256,128)	FusionBlock(256,128)	FusionBlock(256,128)
step 5	-	FusionBlock(128,128)	FusionBlock(128,128)	-	FusionBlock(128,128)
step 6	Upsample	Upsample	Upsample	Upsample	Upsample
step 7	FusionBlock(128,64)	FusionBlock(128,64)	FusionBlock(128,64)	FusionBlock(128,64)	FusionBlock(128,64)
step 8	FusionBlock(64,64)	-	FusionBlock(64,64)	FusionBlock(64,64)	FusionBlock(64,64)
step 9	Decoder	Decoder	Decoder	Decoder	Decoder

TABLE II: Reducing one fusion block in 1-2-2 architecture(The number of fusion blocks from bottom to top) with different orders.

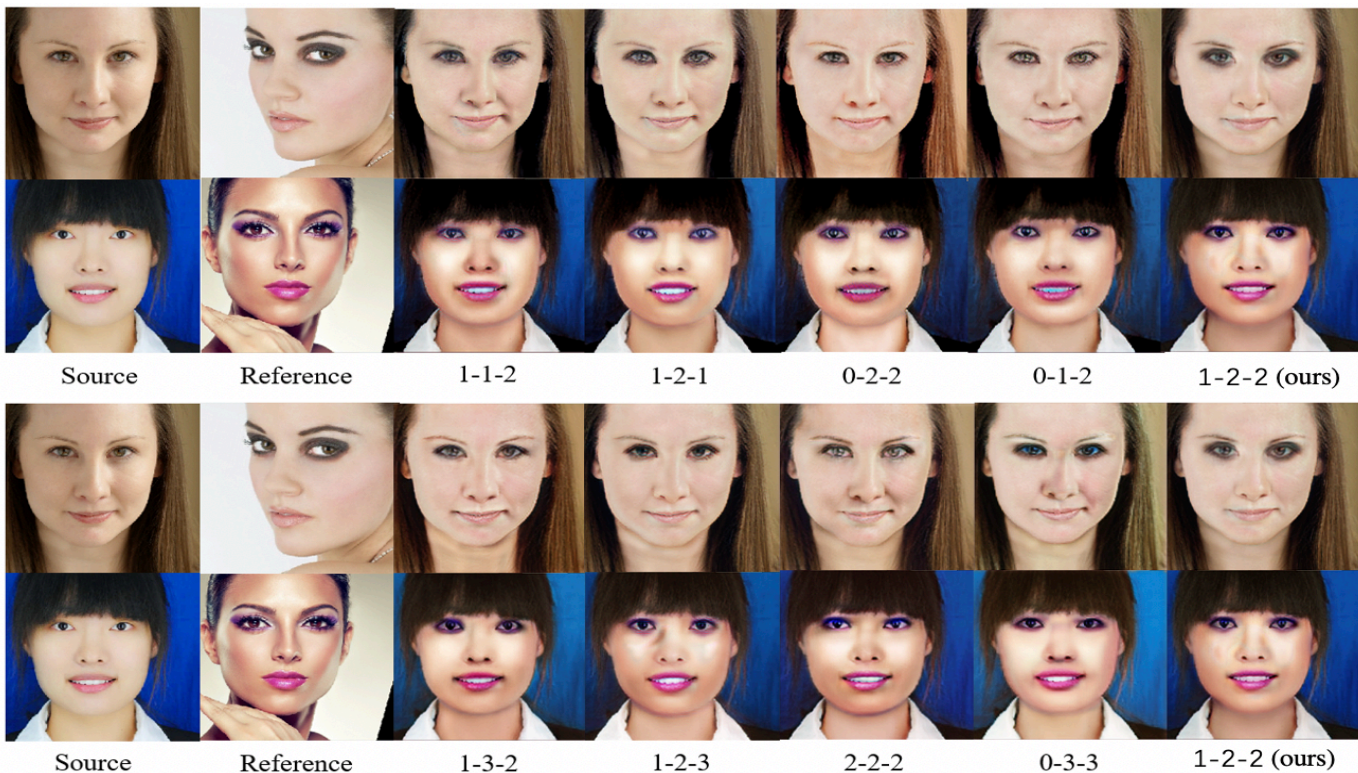


Fig. 1: **Qualitative comparisons with different architectures.** The above two lines show a comparison of different orders for adding a fusion block, while the below two lines show a comparison of different orders for reducing a fusion block.



Fig. 2: **Failure cases in the dataset collected by [?] with complex and dramatic styles.** The transferred texture preservation is not ideal when the reference images have large areas of camouflage or special symbols, then.

Method	SSIM \uparrow	FID \downarrow
beautyGAN[?]	0.8719	55.2437
PSGAN[?]	0.9940	51.2716
SCGAN[?]	0.9918	89.3904
SSAT[?]	0.9922	62.8160
SARA (1-1-2)	0.9895	64.6760
SARA (1-2-1)	0.9890	62.7060
SARA (0-2-2)	0.9885	68.5210
SARA (0-1-2)	0.9891	68.5728
SARA (1-3-2)	0.9895	76.3828
SARA (1-2-3)	0.9900	87.5247
SARA (2-2-2)	0.9900	64.4782
SARA (0-3-3)	0.9904	70.4743
SARA (w/o id)	0.9897	57.3234
SARA (w/o SAM)	0.9899	70.8627
SARA (w/o RAM)	0.9903	63.4023
SARA (full)	0.9900	68.8381

TABLE III: Quantitative comparisons of our method with other methods in terms of SSIM [?] and FID [?]. SARA(1-1-2) refers to an architecture in which the fusion blocks are arranged from bottom to top in a 1-1-2 configuration, while the remaining architectures are similar. SARA (w/o id) denotes without identity loss. SARA (w/o SAM) denotes without spatial-aware alignment module. SARA (w/o RAM) denotes without region-adaptive normalization. They are SARA variants for ablation study. SARA (full) denotes using the full model.



Source Reference BeautyGAN PSGAN SCGAN SSAT EleGANt Ours

Fig. 3: **Qualitative comparisons with open source models in M-Wild dataset.** The compared methods include: **BeautyGAN** [ACMMM'18], **PSGAN** [CVPR'20], **SCGAN** [CVPR'21], **SSAT** [AAAI'22], **EleGANt** [ECCV'22]. SARA is good at handling large misalignment. Detailed analysis are elaborated in Sec ??.